Pharmacological Research - Natural Products 10 (2026) 100578

Contents lists available at ScienceDirect

Pharmacological Research - Natural Products

journal homepage: www.sciencedirect.com/journal/prenap

Comparative spectroscopic analysis of bee propolis: NIR, FT-IR, FT-Raman and ^{1}H NMR. Focus on provenance and antioxidative correlation

Jonas Pordel Vind [a,*], Violetta Aru [b], Henrik Munch Jørgensen [a], Julie Christine Antvorskov [c], Hasim Tekin [a], Knud Josefsen [a], Søren Balling Engelsen [b]

[a] Department of Pathology, The Bartholin Institute, Copenhagen University Hospital, Copenhagen, Denmark
[b] Department of Food Science, University of Copenhagen, Rolighedsvej 26, Frederiksberg, 1958, Denmark
[c] Department of Clinical Research, Steno Diabetes Center Copenhagen, Translational Type 1 Diabetes Research, Herlev, Denmark

ARTICLE INFO

Keywords:
Propolis
Polyphenols
Antioxidative
IR
Raman
NIR
^{1}H NMR

ABSTRACT

Propolis is a polyphenol-rich resinous substance well known for its antioxidative properties. This study describes and compares the chemical composition and radical scavenging activity (RSA) of propolis from Australia (N = 8), Denmark (N = 38), and Norway (N = 7) using infrared (IR), Raman, near-infrared (NIR), and proton nuclear magnetic resonance (^{1}H NMR) spectroscopy through multivariate data analysis. Principal Component Analysis (PCA) showed that Danish and Norwegian propolis samples had a higher content of aromatic compounds, whereas Australian samples were richer in carbohydrates and terpenoids. The RSA of Danish and Norwegian propolis samples was found to be similar ($p \geq 0.05$), while the Australian samples exhibited significantly lower RSA. The strongest spectral correlation ($R^2 = 0.64$) to RSA was found at 1631 cm^{-1} (Raman) and 1666 nm (NIR), attributed to conjugated C=C stretching vibrations and first overtones of C-H stretching vibrations from aromatic/conjugated structures, respectively. NIR spectroscopy provided the most accurate predictions of RSA ($R^2 = 0.75$, RMSECV = 6.66%), highlighting its potential as a rapid, non-destructive quality assessment tool for propolis. Overall, this study demonstrates that the combined use of multiple non-targeted spectroscopic techniques provides complementary insights into complex matrices, enabling a robust characterisation of propolis and its antioxidant activity.

Introduction

Propolis is a natural resinous substance produced by the western honey bee (*Apis mellifera* L.; abbr. *A. mellifera*) to seal and protect the hive from intruders, pathogenic bacteria, fungi, and viruses [1]. Propolis is a mixture of beeswax, plant resins, and glucosidase-containing bee secretions [1–4]. Beeswax is primarily comprised of hydrocarbons and their ester and acid derivatives [5,6]. In contrast, resins are complex mixtures, typically containing terpenoids, and aromatic compounds such as polyphenols [4]. Propolis is well-established to exert an antioxidative effect, and it is widely used in natural medicinal products [7,8]. In literature, the antioxidative properties of propolis are credited to its high concentrations of polyphenols and consequently, most research on the composition of propolis has focused on identifying specific polyphenolic compounds, often employing high-performance liquid chromatography (HPLC) and colorimetric assays [9–11]. Although a targeted identification method provides information about the presence and concentration of selected bioactive compounds, this approach may introduce bias and overlook other potentially important compounds. A more untargeted and unbiased approach to analyzing propolis can be performed using spectroscopic methods such as infrared (IR), Raman, and near-infrared (NIR) spectroscopy, that allow for non-invasive exploratory analysis with minimal or no sample preparation [12]. Proton nuclear magnetic resonance (^{1}H NMR) requires more extensive sample preparation including extraction, but it also delivers inherently quantitative, non-targeted chemical analysis, providing information about the detailed metabolite composition in complex biological mixtures [12]. Overall, the spectroscopic techniques have proven effective not only for assessing polyphenolic content, but also for examining general chemical profiles in propolis, serving as valuable tools for propolis quality control [13–16].

The aim of the present study was to establish an unbiased spectroscopic method to screen propolis, determining its overall chemical composition and predicting its antioxidative activity, expressed as

* Corresponding author.
E-mail address: Jonas.Pordel.Vind@regionh.dk (J.P. Vind).

https://doi.org/10.1016/j.prenap.2026.100578
Received 19 June 2025; Received in revised form 4 February 2026; Accepted 25 February 2026
Available online 27 February 2026

radical scavenging activity (RSA). The study employed several non-targeted spectroscopic methods, including IR, Raman, NIR, and ^{1}H NMR to examine and compare the chemical composition and antioxidative activity in a set of propolis samples (N = 53) from Australia (N = 8), Denmark (N = 38), and Norway (N = 7). ^{1}H NMR data were combined with the data from the vibrational spectroscopic techniques in 2D correlation spectra to aid in signal assignment. Correlation between spectral signals and antioxidative activity was performed. Finally, Partial Least Squares (PLS) regression models [17] were developed to predict the antioxidative activity of propolis from different origins based on the spectroscopic data. To our knowledge, this is the first study to compare and integrate multiple spectroscopic techniques through 2D correlation spectra and multivariate analysis for propolis characterization. The study brings new insights into structure-bioactivity relationships and demonstrates that RSA can be predicted directly from spectral data.

Experimental section

Chemicals

Analytical grade chloroform ($CHCl_3$, ≥99.8%), analytical grade deuterated chloroform ($CDCl_3$, 99%), deuterated dimethyl sulfoxide-d_6 (DMSO-d_6), ferulic acid (99%), HPLC grade caffeic acid (≥98.0%), HPLC grade p-coumaric acid (≥98.0%), NMR grade tetramethylsilane (TMS, ≥99.9%), and 2,2-Diphenyl-1-picrylhydrazyl (DPPH) were purchased from Sigma-Aldrich (Copenhagen, Denmark).

Collection and storage of raw propolis

A total of 53 raw propolis samples were collected from local beekeepers in Australia (N = 8), Denmark (N = 38), and Norway (N = 7). All Danish and Norwegian samples, as well as five of the Australian samples, were obtained from *A. mellifera*. The remaining three Australian samples originated from *Tetragonula carbonaria* (*T. carbonaria*). The differences in bee species for the Australian samples are addressed for each of the relevant analyses described below. Upon arrival, the samples were stored at 4 °C in nitrogen-filled, food-grade ziplock bags placed inside airtight glass containers, also filled with nitrogen. Prior to extraction, liquid nitrogen was applied to the raw propolis, which was then ground into a fine powder using a pestle and mortar.

Propolis extract preparations

Propolis extract preparation for ^{1}H NMR spectroscopy

For each extraction, 100 mg of crushed propolis was mixed with 5 mL of chloroform in round-bottom glass tubes and homogenized for 30 s using a T10 Basic ULTRA-TURRAX ® (IKA-Werke, Germany). After storing in the dark at room temperature for 1 h, the mixture was centrifuged at 3600 RPM for 15 min at 4 °C. After centrifugation, the supernatant (1 mL) was transferred into HPLC vials and left to evaporate overnight in a fume hood. The resulting precipitate was redissolved in 720 μL $CDCl_3$ + TMS (5 mM) and 80 μL DMSO-d_6. Following dissolution, 600 μL of redissolved extract was transferred to an NMR SampleJet tube (Bruker Biospin, Ettlingen, Germany, L = 103.5 mm, D = 5.0 mm) for analysis. Unexpectedly, the Australian samples proved incompatible with the extraction protocol due to high levels of non-dissolvable dispersed solids, which hindered clear and reproducible acquisition of ^{1}H NMR spectra. Several extraction approaches were initially evaluated, including varying concentrations of ethanol and methanol, but none yielded satisfactory reproducibility for the Australian samples (data not shown). However, chloroform provided the best spectral quality and repeatability for the Danish and Norwegian samples (data not shown). It was therefore selected as the standard solvent to ensure consistency across the dataset. Given the distinct chemical profiles of the Australian samples observed from the vibrational spectroscopic analyses and their markedly lower RSA, optimising a separate extraction protocol solely for these samples was considered beyond the scope of this study, particularly as 2D correlations and PLS regression were not feasible for the Australian samples due to their distinct vibrational spectra.

Propolis extract preparation for DPPH RSA assay

Ethanol extracts were prepared following the same approach as described for the extracts prepared for ^{1}H NMR spectroscopy, using ethanol (70%) instead of chloroform, as this approach has proven effective in earlier DPPH RSA studies on propolis [18,19]. After centrifugation, the supernatant (4 mL) was transferred into 15 mL Falcon™ conical centrifuge tubes and stored in a dark cooling room (4 °C) until analysis.

Sample measurements

IR and Raman spectroscopy

IR spectra were obtained using a Bruker Vertex 80 spectrometer equipped with a deuterated triglycine sulfate (DTGS) detector, a potassium bromide (KBr) beam splitter, and a single reflection Platinum Attenuated Total Reflection (ATR) diamond accessory. For Raman measurements, the same instrument was used with a Raman accessory featuring an InGaAs detector and a Nd laser (1065 nm, 200 mW). Both types of spectra were recorded in the range of 500 cm^{-1} to 4000 cm^{-1} with 128 scans per sample. The IR spectra were recorded with a resolution of 4 cm^{-1}, while the Raman spectra were recorded with a resolution of 8 cm^{-1}. IR and Raman spectra were measured in three replicates on raw grounded propolis samples.

NIR spectroscopy

The NIR spectra were measured using the DS2500 analyser (FOSS Analytical A/S, Hillerød, Denmark). The instrument is equipped with a silicon detector (400–1100 nm) and a lead sulfide (PbS) detector (1100–2500 nm). The measurements were collected in the reflectance mode, where the propolis samples were added to a ring cup equipped with a quartz window. The scans were conducted within a wavelength range of 400–2500 nm, with a spectroscopic resolution of 0.5 nm with an average of 8 scans for each sample. NIR spectra were measured in three replicates on raw grounded propolis samples.

^{1}H NMR spectroscopy

Samples included in the study were measured using a Bruker Avance III operating at a proton Larmor's frequency of 600.13 MHz and equipped with a 5-mm broadband inverse (BBI) probe (Bruker Biospin, Rheinstetten, Germany). The magnet was equipped with an automated sample changer (SampleJet™, Bruker Biospin, Rheinstetten, Germany) with a refrigerated storage station (278 K) and heating/drying station (306 K). Cooling of the probe and SampleJet system were controlled by the BCU (Bruker Cooling Unit). Data acquisition and processing were carried out in the TopSpin software (version 3.6, Bruker, Rheinstetten, Germany). Automation of the overall measurement procedure was controlled by the iconNMR™ software (Bruker Biospin, Rheinstetten, Germany). Icon NMR (Bruker Biospin, Germany) was used to control measurement automation. The following parameter setup was employed: 128 scans, a 90° pulse, a 20-ppm sweep width (sw), an acquisition time (aq) of 2.73 s, and a relaxation delay (D1) of 4 s. The ^{1}H NMR spectra were collected into 65 K data points. The receiver gain (RG) value was determined experimentally for each sample. Phase and baseline correction were performed in TopSpin 4.3.0 (Bruker Biospin, Rheinstetten, Germany).

DPPH RSA

The DPPH RSA of propolis ethanol extracts was determined using the DPPH free radical assay [20]. The propolis ethanol extracts were diluted in ethanol to a concentration of 0.5 mg/mL. In a Thermo Scientific™ 96-well conical bottom plate (non-treated surface), 20 μL of each diluted

solution was mixed with 180 μL of a DPPH in ethanol solution (0.1 mM). Positive and negative controls were prepared by mixing 20 μL of ascorbic acid in ethanol (0.5 mg/mL) and 20 μL of ethanol with 180 μL of the DPPH in ethanol solution (0.1 mM), respectively. The 96-well plate was kept in darkness at room temperature for 20 min, after which the absorbance of each well was measured at 517 nm using the CLARIOstar® Plus plate reader (BMG Labtech, Ortenberg, Germany). The DPPH RSA of the propolis samples, relative to the negative control, was used for analysis. RSA values for each sample were calculated as the average of triplicate measurements.

Data analysis

Initial pre-processing of ^{1}H NMR data

The ^{1}H NMR spectra were imported into MATLAB ver. R2023b (MathWorks Inc., Massachusetts, United States) where they were referenced to the TMS singlet at 0.00 ppm. and aligned using *i*coshift [21]. Noisy regions, including the chloroform signal at 7.26 ppm and TMS signal were removed prior to data analysis. The spectra were normalized relative to the RG and mass (mg) of the respective propolis sample.

2D correlation analysis

In this study, 2D correlation spectroscopy plots between vibrational versus ^{1}H NMR spectroscopy and Raman versus NIR spectroscopy [22,23] were generated using covariance calculations in MATLAB (version R2023b). The covariance was calculated using the *cov* function, where XSPEC1 represented the data from one spectroscopic method and XSPEC2 represented the data from another spectroscopic method. In these matrices, rows corresponded to samples and columns represented spectral variables. The vibrational spectroscopy regions for 2D correlation analysis were selected to capture distinct spectral variations relevant to the chemical diversity and the antioxidative activity of the samples. For IR and Raman spectroscopy, this analysis focused on the informative fingerprint region in the 1800–1000 cm^{-1} range which contains all relevant chemical information including carbonyl, ether, ester, acid and aromatic signals. The pure C-H, N-H and O-H stretching (2800–3600 cm^{-1}) proved too unspecific for discriminating between our propolis samples, while the region below 1000 cm^{-1} did not provide useful information, as covariance values were very low and no interpretable features were observed. For NIR spectroscopy, the entire 1100–2500 nm range (PbS detector) was selected for exploring covariations with ^{1}H NMR. IR and Raman spectroscopy data were preprocessed using the Standard Normal Variate (SNV) method [24] to correct for scatter-related intensity variation, followed by Pareto scaling to reduce the dominance of higher intensity signals. NIR data were preprocessed with SNV followed by mean centering. The ^{1}H NMR data were autoscaled prior to analysis to account for the large dynamic range of signal intensities, particularly the highly abundant wax-associated signals. To further improve sensitivity and capture more subtle covariations, the vibrational spectroscopy data were divided into two regions for 2D correlation analysis.

Correlation of spectroscopy data to RSA

For vibrational spectroscopy, the R^2 value was calculated between the maxima of signals attributed to aromatic compounds, as identified in the 2D correlation analysis, and the RSA. For ^{1}H NMR, the average intensity of the aromatic region ($\Delta\delta$ = 6.0–8.5 ppm) was used for correlation analysis. This approach was adopted because the aromatic region of the ^{1}H NMR spectra is densely populated with overlapping signals due to propolis' complex chemical composition, rendering correlations to specific signals unfeasible. Prior to correlation analysis, the IR and Raman data were pre-processed using SNV, while the second derivative was applied to the NIR data. The ^{1}H NMR data were not further pre-processed than beyond the initial processing.

Statistical analysis of DPPH RSA data

For the statistical analysis of DPPH RSA in propolis from different origins, a one-way ANOVA followed by Tukey's HSD test was performed to compare the means among the three groups (Australia, Denmark, and Norway). Although three of the Australian propolis samples were derived from *T. carbonaria* rather than *A. mellifera*, they exhibited no significant difference in RSA and were therefore pooled with the other Australian samples for simplicity.

Multivariate data analysis

Multivariate data analysis was performed with LatentiX 2.13 (LatentiX ApS, Gilleleje, Denmark). For Principal Component Analysis (PCA) [25] the spectral regions analysed were 3600–700 cm^{-1} for IR, 3100–800 cm^{-1} for Raman, 2500–1100 nm for NIR, and the entire recorded spectral range for ^{1}H NMR. The IR, Raman, and NIR data were pre-processed using SNV, to correct for scatter-related intensity variation, followed by mean centering. In contrast, the ^{1}H NMR data were Pareto scaled to reduce the dominance of high-intensity signals while preserving relative metabolite variation. The maximum number of components for PCA was determined using scree plots, resulting in the use of 3 components for the IR and 2 components for the Raman, NIR and ^{1}H NMR data. Higher-order components were also briefly evaluated for all spectroscopic techniques, but they did not improve class discrimination. The Australian samples were again pooled for PCA for simplicity, as the three derived from *T. carbonaria* showed little to no distinction from those of *A. mellifera*. For Partial Least Squares (PLS) regression [26] of the spectral data to the DPPH RSA, the same spectral regions were used for the vibrational spectroscopic techniques as in the PCA. For the ^{1}H NMR data, only the aromatic region ($\Delta\delta$ = 6.0–8.5 ppm) was used, as this provided highest prediction power. The same pre-processing was applied to IR, Raman, and ^{1}H NMR data as in the PCA. NIR data was pre-processed with the second derivative Savitzky-Golay filter and Pareto scaling. The number of latent variables (LVs) for PLS regression was identified based on a plot of Root Mean Square Error of Cross-Validation (RMSECV) versus the number of LVs. This approach led to the selection of one LV for the IR data, two LVs for the Raman and ^{1}H NMR data, and four LVs for the NIR data. Cross-validation was performed using a ten-segment repeated random approach with 25 repetitions, allowing for better representation of the heterogeneity of the propolis samples and reducing the risk of overfitting.

Results and discussion

Introduction to spectroscopic data

The average IR, Raman and NIR spectra for the Australian, Danish and Norwegian propolis samples are presented in Fig. 1A-C. The average ^{1}H NMR spectra for the Danish and Norwegian propolis samples are presented in Fig. 1D. The IR spectra for Danish and Norwegian samples display similar spectroscopic patterns (Fig. 1A), indicating comparable chemical compositions. In contrast, the Australian sample exhibits distinct signals, most notably a broad band around 1040 cm^{-1}. This feature may suggest a higher content of carbohydrates and terpenoids, as it likely arises from overlapping aliphatic C-O and C-O-C stretching vibrations common to both compound classes [27,28]. The propolis samples generally exhibit characteristic IR peaks associated with compounds commonly found in beeswax and resin. Notably, the peaks at 2916 cm^{-1} and 2849 cm^{-1} correspond to the asymmetric and symmetric C-H stretching of aliphatic methylene groups, respectively, which are omni-present in propolis due to the hydrocarbons and its ester and acid derivatives [5]. The carbonyl stretches of the hydrocarbon ester derivatives are observed at 1736 cm^{-1}[5]. Other less pronounced signals include symmetric C-H stretching of aliphatic methyl groups at 2958 cm^{-1}[5] and carbonyl stretching of free fatty acids at 1710 cm^{-1}[29]. The presence of aromatic compounds is suggested by

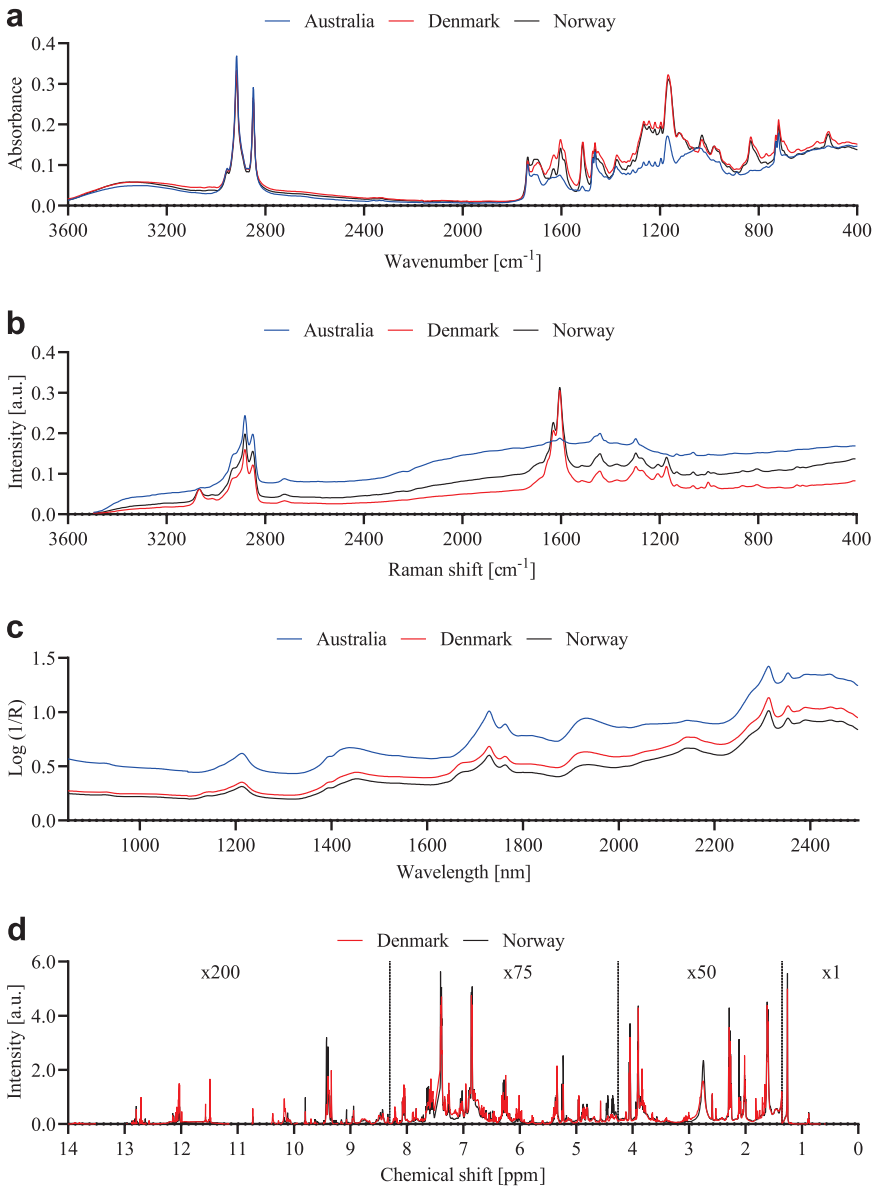

Fig. 1. Average (a) IR, (b) Raman, and (c) NIR spectra for the Australian (N = 8), Danish (N = 38), and Norwegian (N = 7) propolis samples; (d) Average ^{1}H NMR spectra for the Danish and Norwegian propolis samples.

the C═C stretching vibrations appearing in the spectroscopic range of 1610–1510 cm^{-1} [30].

The average Raman spectra (Fig. 1B) also show high similarities between Danish and Norwegian propolis samples, whereas the Australian sample exhibits a distinctly different and more amorphous spectroscopic pattern. Significant fluorescent interference, particularly in the Australian samples, complicates the identification of spectroscopic differences. Nonetheless, in the Raman spectra, the asymmetric and symmetric aliphatic methylene C-H stretches manifest as peaks at 2882 cm^{-1} and 2850 cm^{-1}, respectively [31]. Furthermore, the symmetric C-H stretching of aliphatic methyl groups is observed at 2935 cm^{-1} [31], while the C═C stretches of aromatic compounds are identified at around 1602 cm^{-1} [32].

This brief visual inspection of the IR and Raman spectra already suggests a distinctive chemical profile of the Australian propolis samples compared to the Danish and Norwegian samples. These dissimilarities in chemical composition may reflect differences in the botanical sources and environmental conditions influencing the chemical composition of propolis of different origins.

Fig. 1C presents the average NIR spectra for Danish, Norwegian and Australian propolis samples. While accurate spectroscopic assignment of the NIR spectra is not feasible without supplementary information, the NIR spectra contain substantial information about the chemical composition of the propolis samples through the vibrational combination bands and overtones. In order to elucidate the origins of these, 2D correlation analysis with the ^{1}H NMR data was performed and will be discussed later (Fig. 2).

The ^{1}H NMR spectra (Fig. 1D) of propolis show numerous signals across the spectrum, indicating successful extraction of a wide range of chemically diverse compounds. The most intense signal is observed at $\Delta\delta$ = 1.21 ppm and arises from aliphatic methylene (-CH_2-) protons found primarily in beeswax. The signal appears as a broad singlet, due to the intensity of the prominent protons in hydrocarbons and their ester and acid derivatives [33,34]. Despite the poor baseline resolution due to numerous overlapping signals from the complex chemical composition of propolis, the ^{1}H NMR spectra still provide valuable insights into the proton environments of the compounds present. These spectra not only facilitate the assessment of the types and quantities of compounds

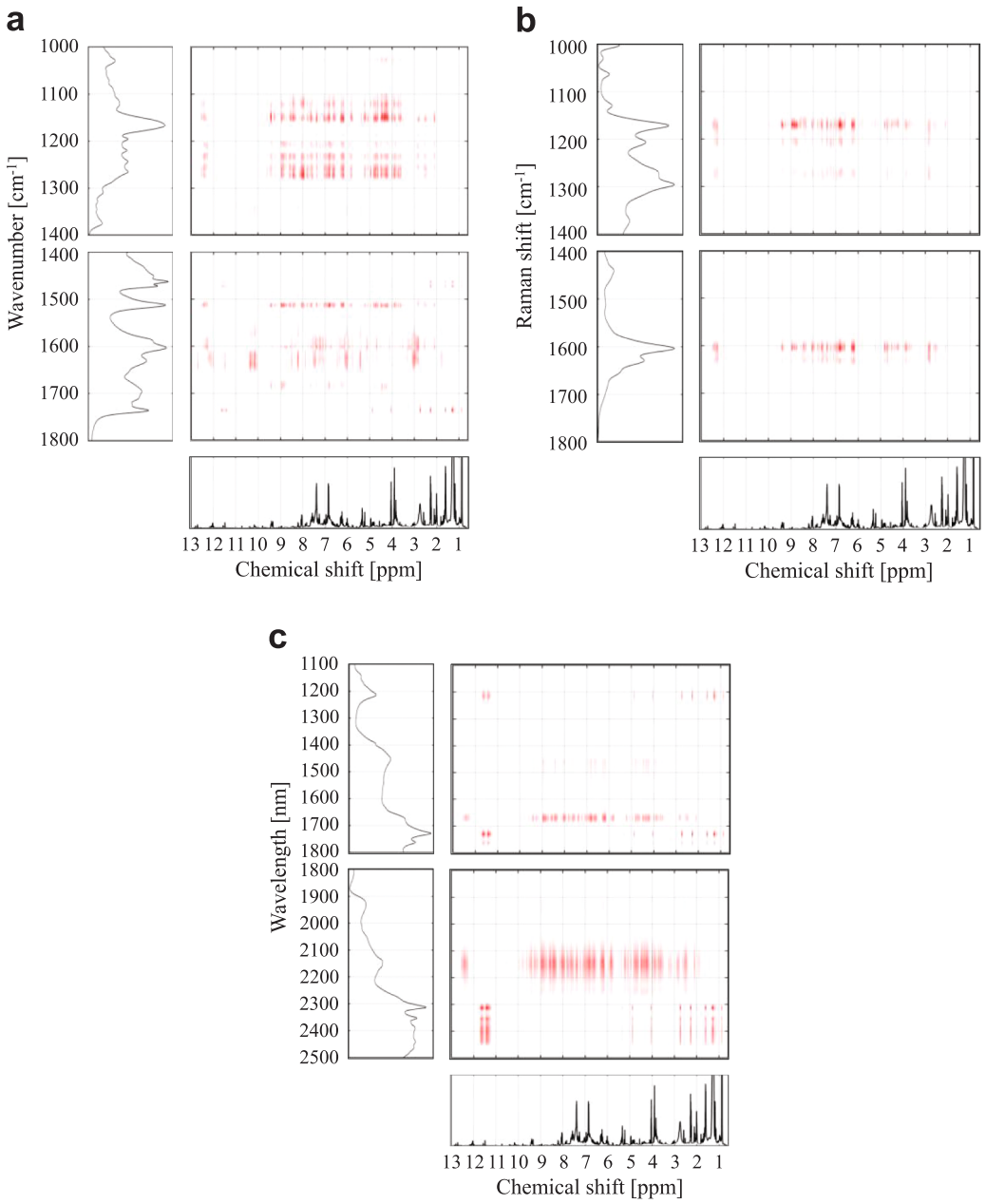

Fig. 2. 2D covariation spectra of (a) IR, (b) Raman, and (c) NIR spectra versus ^{1}H NMR spectra from Danish (N = 38) and Norwegian (N = 8) propolis samples. Preprocessing included Pareto scaling and Standard Normal Variate (SNV) for IR and Raman, mean centering and SNV for NIR, and autoscaling for ^{1}H NMR. The graphics show averaged raw spectra, with the most intense ^{1}H NMR signals truncated for clarity.

within the propolis samples but may also be used to enhance the interpretation of the vibrational spectroscopy data, e.g., IR, Raman, and NIR, by performing 2D correlation spectroscopy [35].

2D correlation spectroscopy and assignment of vibrational spectroscopy signals

To trace the origin of less prominent vibrational spectroscopy signals, potentially linked to antioxidative components, 2D correlation analysis was performed with ^{1}H NMR data. Fig. 2 shows the 2D correlation spectra between IR, Raman, and NIR with ^{1}H NMR. Table 1 summarizes the wavenumber, Raman shift, and wavelength ranges of selected IR, Raman, and NIR signals from raw propolis samples, along with their corresponding vibration modes and putative compounds.

The 2D correlation analysis of IR (Fig. 2A), Raman (Fig. 2B), and NIR (Fig. 2C) with ^{1}H NMR revealed distinct patterns of covariation. Vibrational spectroscopy signals associated with the aromatic region of the ^{1}H NMR spectrum ($\Delta\delta$ = 6.0–8.5 ppm) covary with a wide range of other ^{1}H NMR signals, suggesting co-occurrence of diverse resin-derived non-aromatic compounds. In contrast, vibrational signals linked to the aliphatic methylene signal at $\Delta\delta$ = 1.21 ppm in the ^{1}H NMR spectrum show no covariation with aromatic protons, indicating a clear separation between beeswax and resin components. Several IR signals covary with the aromatic region of the ^{1}H NMR spectrum (Fig. 2A). These signals may be attributed to aromatic C═O stretches (1695–1688 cm^{-1}) [39], aromatic/conjugated C═C stretches (1655–1510 cm^{-1}) [30], and aromatic C-O and C-O-C stretches (1374–1160 cm^{-1}) [30,39]. Signals ranging between 1124 and 1100 cm^{-1} seemingly also correlates strongly with the aromatic region, however, this region is often attributed to aliphatic C-O and C-O-C stretches and likely arise from carbohydrates and terpenoids found in resin. Signals at 1736–1710 cm^{-1} have

Table 1
Spectral regions from IR, Raman, and NIR analyses of raw propolis, along with corresponding vibrational modes and suspected compounds.

IR, Raman, and NIR spectroscopy of crude propolis			
IR			
Wavenumber (cm^{-1})	**Vibration Mode**	**Suspected compounds**	**Ref.**
3500–3100	ν(O-H)	Polyphenols, carbohydrates	[36]
3065	ν(C-H) (aromatic)	Polyphenols	[37]
3020	ν(C-H) (olefinic)	Terpenoids	[37]
2958–2849	$\nu_s(CH_3)$, $\nu_{as/s}(CH_2)$ (aliphatic)	Wax	[5]
1736	ν(C═O) (ester)	Wax	[38]
1710	ν(C═O) (carboxylic acid)	Wax	[38]
1695–1688	ν(C═O) (conjugated)	Polyphenols	[39]
1655–1620	ν(C═C) (conjugated)	Polyphenols	[30]
1610–1510	ν(C═C) (aromatic)	Polyphenols	[30]
1471–1450	$\delta_{ip}(CH_2)$ (aliphatic)	Wax	[5]
1374–1160	ν(C-O), ν(C-O-C) (aromatic)	Polyphenols	[30, 39]
1124–1000	ν(C-O), ν(C-O-C)	Carbohydrates, terpenoids	[27]
Raman			
Raman shift (cm^{-1})	**Vibration Mode**	**Suspected compounds**	**Ref.**
3068	ν(C-H) (aromatic)	Polyphenols	[30]
3018	ν(C-H) (olefinic)	Terpenoids	[31]
2935–2850	$\nu_s(CH_3)$, $\nu_{as/s}(CH_2)$ (aliphatic)	Wax	[31]
1655–1630	ν(C═C) (conjugated)	Polyphenols	[30]
1600–1605	ν(C═C) (aromatic)	Polyphenols	[30]
1445	δ_{ip}(C-H) (aliphatic)	Wax	[31]
1294–1170	δ_{ip}(C-H) (aromatic)	Polyphenols	[32]
NIR			
Wavelength (nm)	**Vibration mode**	**Suspected compounds**	**Ref**
2445–2310, 1416–1390	Combination bands (aliphatic)	Wax	[40]
2170–2130	Combination bands (aromatic)	Polyphenols	[41]
1940–1900	Combination bands (O-H)	Carbohydrates, terpenoids, polyphenols	[42]
1765–1730	2ν(C-H) (aliphatic)	Wax	[40]
1680–1665	2ν(C-H) (aromatic/ conjugated)	Polyphenols	[41]
1450	2ν(O-H)	Carbohydrates, terpenoids, polyphenols	[42]
1215	3ν(C-H) (aliphatic)	Wax	[43]

Keys: $\nu_{as/s}$, asymmetric/symmetric stretching; δ_{ip}, in-plane bending; 2ν, first overtone; 3ν, second overtone

been previously assigned to carbonyls of hydrocarbons derivatives of beeswax and they also covary with characteristic wax signals observed in the ^{1}H NMR spectra (e.g., at $\Delta\delta = 1.21$ ppm). The same is observed for IR signals at 1471–1462 cm^{-1} , arising due to in-plane bending of aliphatic C-H groups [5,44]. In contrast to IR, no covariation was observed between the Raman and ^{1}H NMR signals originating from beeswax in the selected spectral region (Fig. 2B). However, several Raman signals exhibited covariation with the aromatic region of the ^{1}H NMR spectra. These signals include those at 1655–1600 cm^{-1} (aromatic/conjugated C═C stretches) and 1294–1170 cm^{-1} (in-plane bending of aromatic C-H).

The 2D correlation analysis of the NIR and ^{1}H NMR spectra reveal the origin of several of the observed NIR signals (Fig. 2C). The covariation with ^{1}H NMR signals originating from beeswax suggests that the signals at wavelengths 2314–2443 nm and 1390–1416 nm may correspond to combination bands arising from the vibrations of aliphatic compounds in beeswax [40]. The first and second overtones of these compounds are likely observed at 1730–1765 nm and 1215 nm, respectively [43]. NIR signals exhibiting covariation with the aromatic region include signals at 2130–2170 nm (combination bands) [40] and 1665–1680 nm (first overtones) [41], although the latter range cannot be definitively attributed to aromatic or conjugated C-H and is discussed in detail later (Fig. 5). Signals observed at 1900–1940 nm and 1450 nm also weakly exhibit covariation with the aromatic region, however, these are more likely to originate from the combination bands and first overtones of hydroxyl groups found primarily on carbohydrates, terpenoids, and polyphenols [42], and will be discussed further later (Fig. 3C). The separation of resin- and beeswax-derived features in the IR and NIR 2D correlations indicates that the analysis primarily reflects differences in the overall resin-to-wax ratio. As a result, resin signals tend to covary with other resin-associated signals, while beeswax features covary within a narrower aliphatic domain. Although such covariance does not imply that a single compound gives rise to all correlated signals, it is valuable for distinguishing the chemical origin of bands. Notably, this differentiation is also biologically relevant, as the resin fraction contains the aromatic and polyphenolic constituents responsible for antioxidant activity, whereas beeswax would be expected to contribute minimally.

Principal component analysis of the propolis samples

To further investigate the chemical differences among the propolis samples, PCA was employed to analyse spectral patterns and sample variability. Fig. 3 presents the scores and loadings plots from the PCA of IR, Raman, NIR, and ^{1}H NMR spectroscopy data for the propolis samples. For IR, Raman, and NIR all replicate measurements are shown in the PCA, while there were no technical replicates for ^{1}H NMR. Two Danish samples were excluded from the ^{1}H NMR PCA analysis because their spectra indicated faulty extraction process. For all vibrational spectroscopic methods, the scores plot shows substantial inter-sample variability with a clustering of the Australian samples, distinct from the Danish and Norwegian samples (Fig. 3A-C). However, no clear differentiation between the Danish and Norwegian samples is observed in any of the four spectroscopic methods (Fig. 3A-D). Notably, the IR and Raman scores plots also demonstrate considerable intrasample (replicate) variability, whereas the NIR scores plot shows comparatively lower variability.

In the IR scores plot (Fig. 3A), no apparent discrimination based on sample origin is seen along PC#1. The loadings plot for PC#1 shows that this component primarily distinguishes the samples based on signals from wax (negative loadings at 2916 and 2849 cm^{-1}) and, to a lesser extent, aromatic compounds (positive loadings at 1603 and 1512 cm^{-1}). However, the clustering of Australian samples relative to Danish and Norwegian samples is explained along PC#2. For PC#2, negative loadings are primarily attributed to signals in the region of 1265–1160 cm^{-1} (C-O and C-O-C stretches of polyphenols) and the signal at 1512 cm^{-1} (aromatic C═C stretches). In contrast, positive loadings are dominated by signals in the region of 1105–880 cm^{-1}, attributed to C-O and C-O-C stretches of carbohydrates and terpenoids. Furthermore, the broad signal with a maximum around 3300 cm^{-1}, attributed to O-H stretching vibrations (Table 1), also contributes to the positive loadings, suggesting that these O-H stretches predominantly originate from carbohydrates and terpenoids rather than polyphenols. The IR data, therefore, suggests no differentiation in wax content based on the origin of the propolis samples. However, Danish and Norwegian propolis appear to contain higher amounts of polyphenols, while Australian propolis has a higher carbohydrate and terpenoid content.

The Raman scores plot (Fig. 3B) shows no clear clustering of the Australian and Danish/Norwegian samples based on any single principal component. However, when considering both PC#1 and PC#2 together, the Australian samples appear to cluster in the upper left quadrant (negative PC#1 and positive PC#2). PC#1 is primarily influenced by signals from polyphenols (positive loadings at 1631 and 1602 cm^{-1}) and wax (negative loadings at 2882 and 2848 cm^{-1}). Similarly, these signals also drive the loadings for PC#2, where both contribute negatively. The clustering of Australian samples in the upper left quadrant thus aligns with the findings from IR spectroscopy (Fig. 3A), supporting the conclusion that Danish and Norwegian propolis samples contain higher

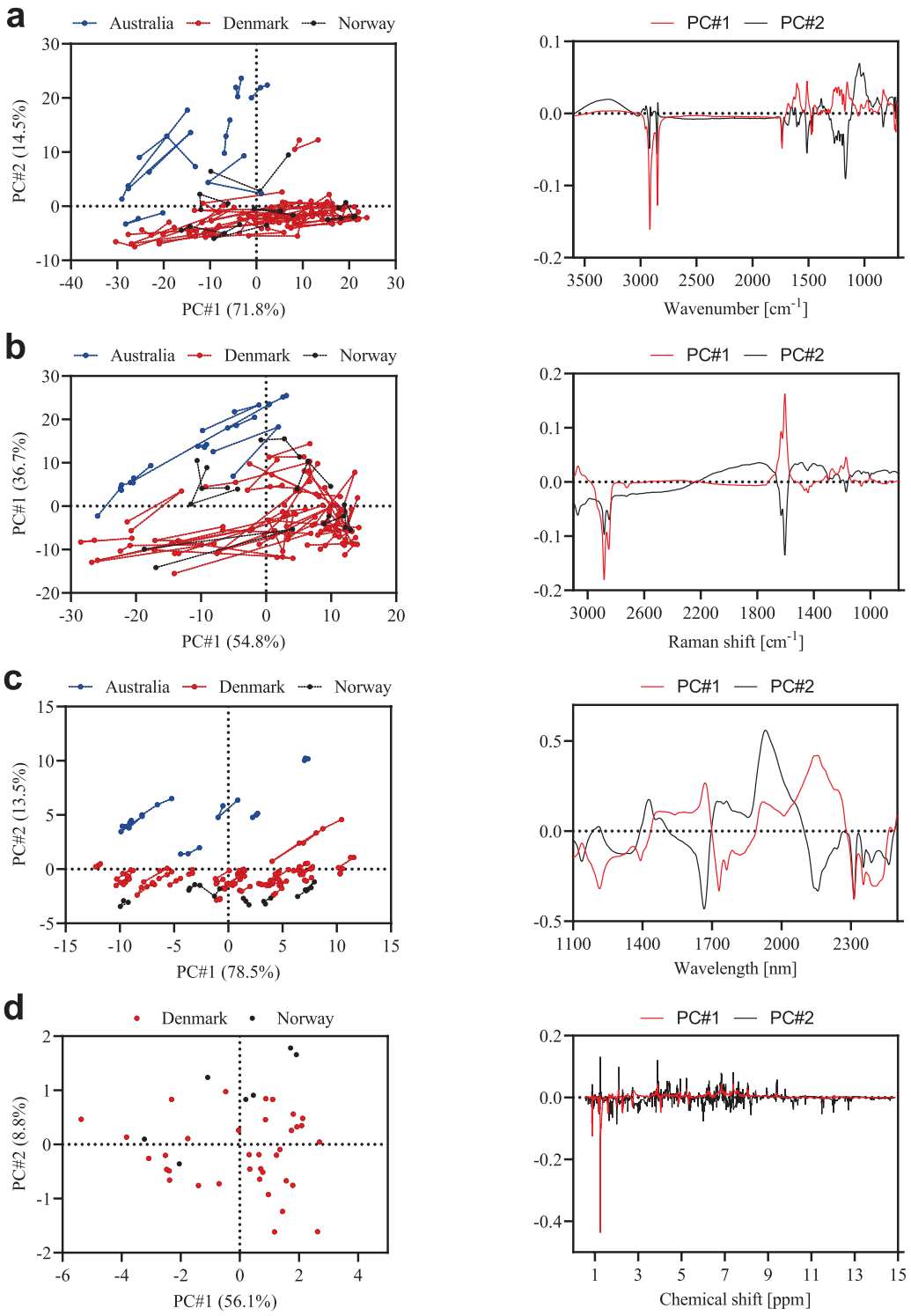

Fig. 3. PCA scores plots (left) and corresponding loadings plots (right) for (a) IR, (b) Raman shift, and (c) NIR measurements of Australian (N = 8), Danish (N = 38), and Norwegian (N = 7) propolis samples, and (d) ^{1}H NMR measurements of Danish and Norwegian propolis samples. Replicates for IR, Raman, and NIR (n = 3) are connected by stippled line.

amounts of aromatic compounds.

The NIR scores plot reveals a similar sample differentiation pattern to the IR scores plot, with the clustering of Australian samples driven by PC#2 rather than PC#1. PC#1 is primarily influenced by signals attributed to beeswax, including combination bands (2310–2445 nm) and overtones (1730–1765 nm, 1215 nm), which contribute to the negative loadings. In contrast, positive loadings are associated with signals from aromatic/conjugated compounds (2130–2170 nm, 1665–1680 nm). Signals ascribed to combination bands of hydroxyl-containing compounds (1900–1940 nm) also contribute positively to PC#1, albeit to a lesser extent. In contrast, these hydroxyl-related signals strongly drive the positive loadings for PC#2. The negative loadings for PC#2 are primarily driven by signals attributed to combination bands of either wax (2310–2445 nm) or aromatic compounds (2130–2170 nm), as well as the first overtones of aromatic/conjugated compounds (1665–1680 nm). The differentiation between signals

associated with aromatic and hydroxyl-containing compounds is particularly noteworthy. Although some aromatic compounds, such as polyphenols, include hydroxyl moieties, carbohydrates and terpenoids also contribute significantly to this functional group. The differentiation observed in PC#2, further supported by the PCA of IR data, suggest that these hydroxyl-related signals primarily originate from carbohydrates and terpenoids rather than polyphenols. This interpretation indicates that the PCA of NIR data highlights not only the lower concentration of aromatic compounds in Australian samples (as corroborated by IR and Raman data) but also their higher carbohydrate and terpenoid content, which drives their distinct clustering. Furthermore, the aforementioned comparatively larger intra-sample variability observed in the IR and Raman scores plots, relative to NIR, may be explained by NIR's superior ability to sample heterogeneous materials. Its larger sampling area and volume allow for more representative analysis, resulting in more robust chemical information [45]. The larger intra-sample variation observed for the IR and Raman data is primarily due to the small sample size measured, which, combined with the heterogeneous samples, contribute to replicate variability. In Raman spectroscopy, sample presentation can be influenced by varying sample fluorescence, whereas in IR spectroscopy it can be influenced by sample contact to the ATR crystal. To minimise these effects, measurements including replicates were performed in randomised runs under standardised acquisition settings.

Like for the vibrational spectroscopy, the ^{1}H NMR scores plot (Fig. 3D) does not reveal any chemical differences between the Danish and Norwegian samples. The negative loadings for PC#1 are primarily driven by signals in the aliphatic region, such as the aliphatic methylene signal at $\Delta\delta = 1.21$ ppm arising from wax, while the positive loadings are driven, to a lesser extent, by signals from the aromatic region ($\Delta\delta =$ 6.0–8.5 ppm). Variation along PC#2 appears to be primarily influenced by signals associated with wax (negative loadings). However, contributions from other spectral regions are less distinct, indicating potential variability in the chemical composition that remains unexplained. In summary, all employed vibrational spectroscopy techniques demonstrated a clear distinction between the Australian propolis samples compared to the Danish and Norwegian samples, primarily based on their aromatic content. Additionally, IR and NIR spectroscopy suggested that the Australian samples contained higher levels of carbohydrates and terpenoids relative to the Danish and Norwegian samples. This strongly indicates that the chemical composition of propolis is highly dependent on geographical location and the available flora for resin collection.

DPPH radical scavenging activity of propolis

To validate the PCA findings on differences in aromatic content, the antioxidative activity of the propolis samples was assessed using the 2,2-Diphenyl-1-picrylhydrazyl (DPPH) Radical Scavenging Activity (RSA) assay [46]. Since aromatic compounds, such as polyphenols, are major contributors to the antioxidant activity of propolis, the RSA serves as a relevant metric for this analysis. Fig. 4 presents a country-grouped boxplot showing the RSA of propolis samples from Australia, Denmark, and Norway.

Based on a one-way ANOVA followed by Tukey's HSD test, the RSA of the Danish and Norwegian samples showed no significant difference ($p \geq 0.05$), whereas the Australian samples exhibited significantly lower RSA compared to both the Danish ($p < 0.0001$) and Norwegian ($p < 0.001$) samples. This similarity in RSA between the Danish and Norwegian samples aligns with the spectral PCA results, which revealed no clear chemical distinction between them. In contrast, the PCA indicated that the Australian samples differed chemically from the others, primarily due to their lower aromatic content. As RSA is largely influenced by the aromatic content of a sample, these PCA findings are consistent with the observed RSA differences. Notably, one Danish sample appeared as an outlier, exhibiting a comparatively lower RSA, which was not expected based on the PCA. This highlights that the antioxidant capacity of propolis may vary substantially even within a single geographic origin and could depend on factors not fully represented in the PCA.

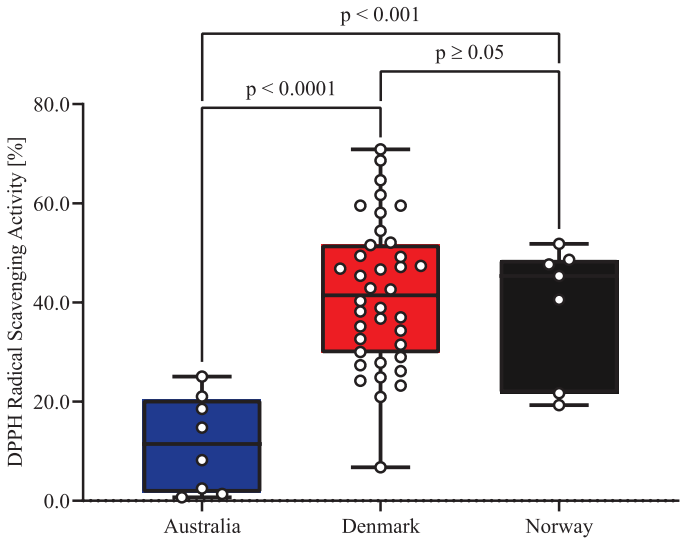

Fig. 4. Country-grouped boxplot displaying the 2,2-Diphenyl-1-picrylhydrazyl (DPPH) radical scavenging activity (RSA) of propolis samples from Australia (N = 8), Denmark (N = 38), and Norway (N = 7) relative to the negative control. White dots represent the average RSA of triplicates for each sample.

Correlation of spectroscopic signals to DPPH radical scavenging activity

To further explore the relationship between vibrational spectroscopy data and antioxidant activity, the correlation between spectral signals and the measured RSA was examined. The Australian samples were excluded due to their distinct spectral features compared to the Danish and Norwegian samples.

R^2 values were calculated between RSA and vibrational spectroscopic signals associated with aromatic compounds, specifically those covarying with the aromatic region shown in Fig. 2. For ^{1}H NMR, the average signal intensity in the aromatic region was used for correlation with RSA. The highest correlation (Table 2) was observed with similar magnitude ($R^2 = 0.64$) in both the Raman and NIR spectra at 1631 cm^{-1} and 1666 nm, respectively. The tentative assignment of these bands will be discussed later in Fig. 5. The aromatic region of ^{1}H NMR showed a

Table 2
Spectral variables, their respective vibration modes (as presented in Table 1) or signal origin, and Pearson's correlation coefficients to the 2,2-Diphenyl-1-picrylhydrazyl (DPPH) Radical Scavenging Activity (RSA) (Fig. 4). Preprocessing techniques included standard normal variate (SNV) for IR and Raman data, and the second derivative for NIR data, while no preprocessing was applied to the ^{1}H NMR data. For ^{1}H NMR, the average signal intensity of the aromatic region (6.0–8.5 ppm) was used for correlation analysis.

Technique	Identified Variable	Vibration mode/origin of signal	R^2 to RSA
IR	1232 cm^{-1}	ν(C-O), ν(C-O-C) (aromatic) [30, 39]	0.55
	1273 cm^{-1}	ν(C-O), ν(C-O-C) (aromatic) [30, 39]	0.52
Raman	1602 cm^{-1}	ν(C═C) (aromatic) [30], Fig. 5	0.58
	1631 cm^{-1}	ν(C═C) (conjugated) [30], Fig. 5	0.64
NIR	1666 nm	2ν(C-H) (aromatic/conjugated) [41], Fig.5	0.64
	1678 nm	2ν(C-H) (aromatic/conjugated) [41], Fig. 5	0.62
^{1}H NMR	6.0–8.5 ppm	Aromatic protons	0.58

Keys: ν; stretching, 2ν, first overtone

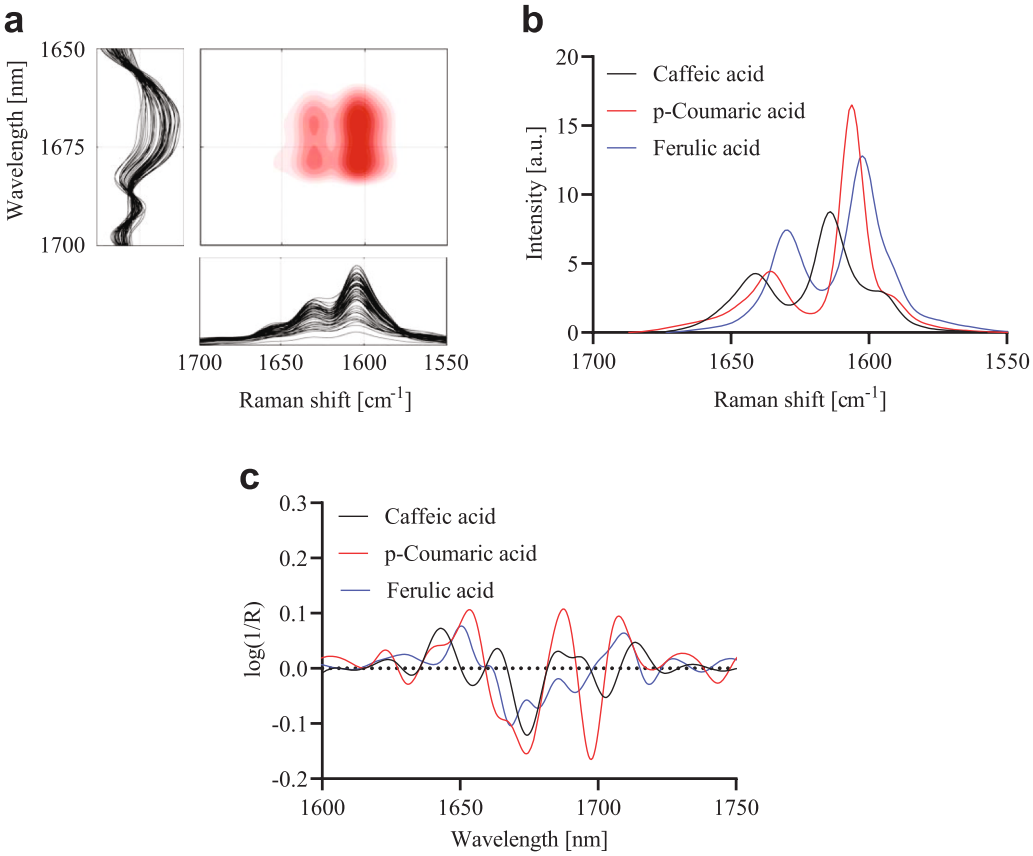

Fig. 5. (a) 2D covariation spectra of Raman (1700–1550 cm^{-1}) and NIR (1650–1700 nm) regions showing the highest correlations with RSA (Table 2). Raman data were pre-processed using standard normal variate (SNV) and Pareto scaling, while NIR data were treated with a second-derivative Savitzky-Golay filter and mean centering. Raw Raman and second-derivative NIR spectra are shown for Danish (N = 38) and Norwegian (N = 7) samples. (b) Raman and (c) second-derivative NIR spectra of selected regions for model compounds: caffeic acid, *p*-coumaric acid, and ferulic acid.

slightly lower correlation (R^2 = 0.58), while IR exhibited the weakest correlations among the four spectroscopic methods, with the signal at 1232 cm^{-1} yielding an R^2 value of 0.55.

The observed differences in correlation may be attributed to the principles underlying each technique. Raman spectroscopy, which is sensitive to changes in polarizability [47], is particularly responsive to C═C stretches of non-conjugated, conjugated and aromatic compounds. Given that antioxidant activity in propolis is largely driven by aromatic systems with the ability to stabilise radicals through hydrogen or electron donation, this sensitivity likely contributes to the strong correlation with RSA. In contrast, NIR spectroscopy allows for optimal sampling of heterogeneous samples due to its larger sampling area and volume as mentioned earlier [45]. While unprocessed NIR signals are typically broader and less specific, applying a second derivative enhances spectral resolution by reducing baseline effects and sharpening overlapping peaks [48]. This may improve sensitivity to aromatic structures and increase the specificity of signals, making NIR data more reliable for correlation analysis. IR spectroscopy, which is sensitive to changes in dipole moments [49], is particularly effective for detecting the stretching of polar bonds such as C-O and C-O-C. The signal observed at 1232 cm^{-1} has previously been attributed to these bonds. The slightly lower correlation observed for IR may result from its sensitivity to functional groups that do not directly contribute to antioxidant activity. Although such polar bonds may be present in aromatic compounds, the antioxidant activity of propolis is more strongly linked to conjugated C═C systems, which are more effectively detected by Raman spectroscopy. ^{1}H NMR showed a moderate correlation with RSA, reflecting the contribution of aromatic protons. However, averaging the entire aromatic region may dilute specificity, as signals from non-antioxidative compounds could also be present.

To support the assignment of the Raman and NIR signals showing the highest R^2 values to RSA, additional analysis was performed using 2D correlation spectroscopy (Fig. 5A). Furthermore, Raman and NIR spectra were recorded for three model compounds commonly found in propolis [50]: caffeic acid, p-coumaric acid, and ferulic acid, all of which contain both aromatic and conjugated C═C bonds. These measurements were used to aid in final signal assignment, and the relevant spectral regions are shown in Fig. 5B-C.

The 2D correlation spectrum (Fig. 5A) reveals covariation between the Raman and NIR signals of interest, consistent with their shared correlation with RSA. In the Raman spectrum, two distinct signals at 1602 and 1631 cm^{-1} are observed. While relatively well-resolved, these signals remain broad, suggesting potential overlap from multiple contributing aromatic compounds. In contrast, the NIR signals are notably broader and less distinguishable, indicating a higher degree of spectral overlap in this region. Nevertheless, two signals at wavelengths 1666 and 1678 nm exhibit stronger covariation with the Raman signal at 1631 cm^{-1} than other wavelengths in the selected region, aiding in the identification of the variables of interest.

The Raman spectra of the model compounds (Fig. 5B) also display both signals observed in Fig. 5A, although their exact peak positions and intensities vary among the compounds. Since these compounds differ only in the substituents on the benzene ring, specifically the presence or absence of a methoxy group and the different positioning of hydroxyl groups, this variation likely reflects the influence of electronic effects, particularly resonance and conjugation, on the electron distribution within the aromatic system and the associated C═C vibrational modes. The presence of both the 1631 and 1602 cm^{-1} signals across all three

compounds supports their assignment to distinct vibrational origins. The 1602 cm^{-1} signal is likely associated with aromatic C=C stretches within the benzene ring, reflecting lower energy and delocalized π-electrons. In contrast, the 1631 cm^{-1} signal is more plausibly attributed to conjugated (non-aromatic) C=C stretches, which typically resonate at slightly higher energy due to their more localized electronic structure.

The NIR spectra of the model compounds (Fig. 5C), by comparison, are more ambiguous. Application of the second-derivative Savitzky-Golay filter reveals several overlapping bands, which likely originate from the first overtones of aromatic and/or conjugated C-H stretches. However, unlike the Raman spectra, it is not feasible to distinguish which signals arise from aromatic versus conjugated C-H overtones in the NIR spectra of the model compounds, and by extension, in those of the propolis samples. This limitation stems primarily from the overlapping nature of these overtones and is further compounded by the extensive spectral congestion in the NIR region of the propolis samples, reflecting their inherently complex, polyphenol-rich composition. Although exact determination of the origin of these signals is not realistic, the 2D correlation analysis (Fig. 5A) helps to lessen this ambiguity by highlighting the two NIR bands, at 1666 nm and 1678 nm, that covary with the Raman signal at 1631 cm^{-1}. These findings underscore the relevance of these NIR features despite the spectral complexity and support their association with vibrational modes of aromatic and/or conjugated structures. Notably, the NIR peaks of the model compounds appear at slightly higher wavelengths compared to those in the propolis spectra. This discrepancy may be attributed to matrix effects, as the resinous nature of propolis could influence how compounds interact with the light source, potentially shifting their absorbance features.

Together, these results highlight how the different spectroscopic methods complement one another in providing insight into the chemical composition of propolis. Each method offers distinct advantages and limitations, with varying sensitivity and specificity toward the antioxidant-relevant structures in propolis.

Prediction of radical scavenging activity based on spectroscopic data

In order to scrutinize the relation between the chemical spectra and the RSA, a PLS regression model was created to evaluate the ability of the applied spectroscopic techniques to predict the RSA of the propolis samples. Due to the large replicate variability of IR and Raman measurements, observed in the PCA (Fig. 2), an average of the triplicates was used for PLS regression. The Australian samples were excluded from the analysis due to their distinct chemical composition and lower aromatic

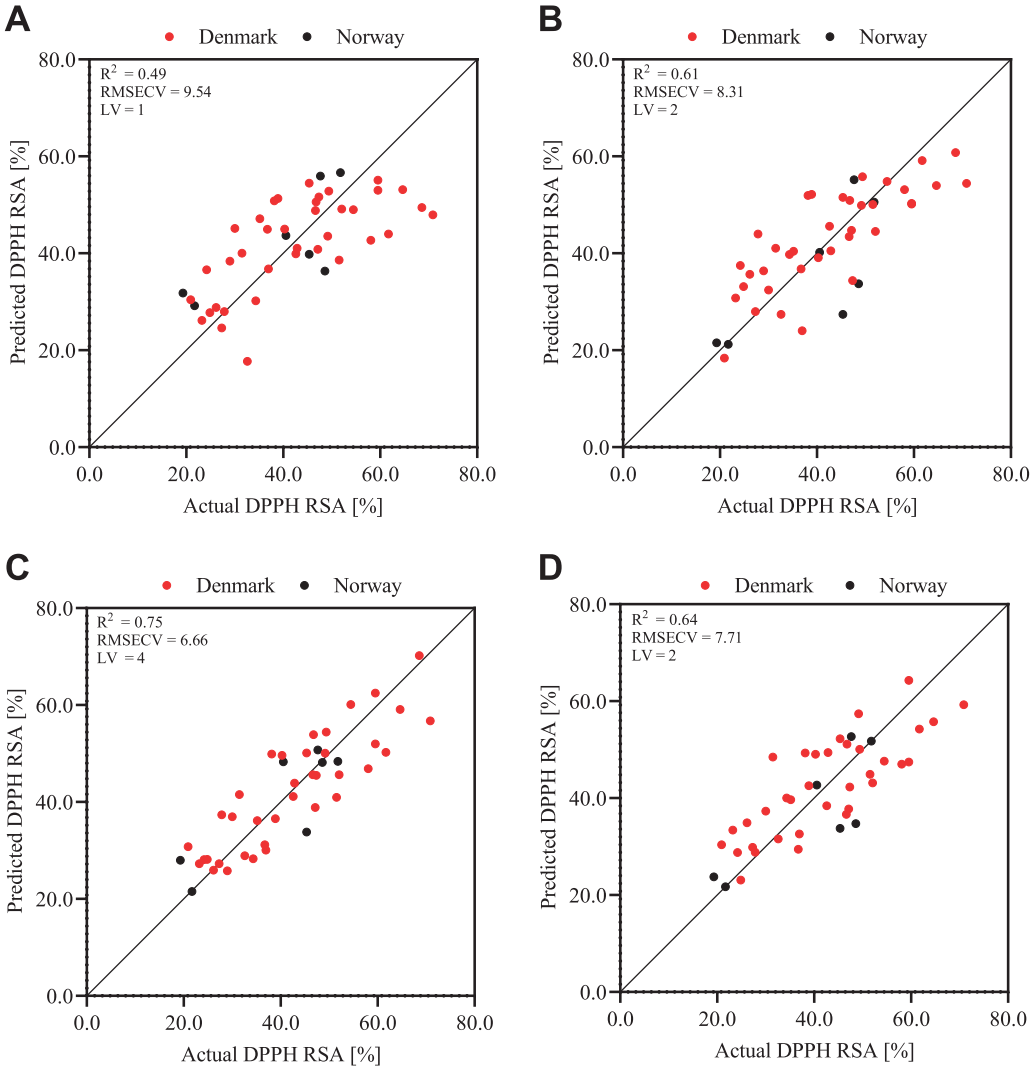

Fig. 6. Actual versus predicted plots for the (2,2-Diphenyl-1-picrylhydrazyl) DPPH Radical Scavenging Activity (RSA) of Danish (N = 37) and Norwegian (N = 7) propolis samples based on (a) IR, (b) Raman, (c) NIR, and (d) ^{1}H NMR data. The observed R^2 values for IR, Raman, NIR, and ^{1}H NMR data were 0.49, 0.61, 0.75, and 0.64, respectively, with corresponding respective Root Mean Square Error of Cross-Validation (RMSECV) values of 9.54%, 8.31%, 6.66%, and 7.71%. The latent variables (LV) for the IR, Raman, NIR, and ^{1}H NMR models were 1, 2, 4, and 2, respectively.

content, both of which are key determinants of RSA and could potentially obscure the relationship between chemical spectra and RSA in the Danish and Norwegian samples. In addition, the Danish sample previously identified as an RSA outlier was omitted from the spectroscopic models. For the ^{1}H NMR model, two additional samples previously associated with extraction errors were also excluded. These omissions were made to ensure a more robust and accurate evaluation of the PLS models. Fig. 6 shows the actual versus predicted plot of the RSA as predicted by the four spectroscopic-based PLS regression models.

The NIR-based model exhibited the best predictive power with R^2 and Root Mean Square Error of Cross-validation (RMSECV) values of 0.75 and 6.66%, respectively. The Raman-based model (R^2 = 0.61, RMSECV = 8.31%) and the ^{1}H NMR-based model (R^2 = 0.64, RMSECV = 7.71%) demonstrated similar predictive performance, while the IR-based model produced the worst predictive power (R^2 = 0.49, RMSECV = 9.54%). Thus, NIR proved to have the highest predictive power, likely explained by the much better sampling of heterogeneous samples by this method. The relatively high predictive power of Raman spectroscopy and ^{1}H NMR compared to IR for predicting RSA likely stems from their sensitivities to key molecular features, as discussed earlier. Raman spectroscopy is particularly effective at detecting aromatic/conjugated C=C stretching vibrations due to the changes in polarization, which are fundamental functional groups to antioxidative activity. Similarly, ^{1}H NMR provides detailed insights into proton environments, recording significant information about functional groups and molecular interactions that may influence RSA. In contrast, the lower performance of IR spectroscopy may result from its focus on dipole moment changes rather than polarization, as well as potential limitations associated with triple-bounce diamond ATR sampling.

However, a direct comparison between the vibrational spectroscopy-based models and the ^{1}H NMR-based model may not be entirely valid, as ^{1}H NMR analysis requires sample extraction prior to measurement, whereas vibrational spectroscopic methods can analyse the sample directly. The extraction step inherently increases the risk of biased errors, as evidenced by the two excluded outliers linked to issues during the extraction process. Furthermore, the analysis is also subsequently limited to the extracted components, potentially omitting compounds present in the crude sample. Consequently, the broader compositional overview offered by vibrational spectroscopy may be advantageous in certain contexts, with NIR being particularly well-suited for sampling of heterogeneous materials. Despite this fundamental limitation, liquid state ^{1}H NMR still offers the advantage of providing more detailed molecular information of complex biological samples compared to vibrational spectroscopic methods, allowing for more precise identification of specific chemical compounds. Therefore, when choosing a spectroscopic method, it is crucial to consider the strengths and limitations of each technique in relation to the analysis goals and recognize that they can all provide complementary information.

Limitations of this study include the small number of Australian samples and their exclusion from the ^{1}H NMR analysis, which weakens conclusions for this group and limits regional generalisability. Although repeated cross-validation ensured robust model performance, our limited sample set did not allow for an external validation set. Future studies should include independent datasets from other geographical regions to confirm the predictive performance and broader applicability of the models. A further limitation of the present study is that the applied spectroscopic approaches do not allow comprehensive chemical typing of propolis or unambiguous identification of individual compounds. While vibrational spectroscopic techniques provide rich information on overall chemical features and structural classes, they do not resolve the specific molecular constituents traditionally used to define propolis types. Although ^{1}H NMR has the potential to deliver more detailed molecular information, extensive signal overlap from aromatic protons within the chemically complex propolis matrix precluded confident compound-level identification in the present dataset. Consequently, the findings should be interpreted as functional and compositional fingerprints rather than exhaustive chemical characterizations. From a quality control perspective, this fingerprint-based strategy remains highly relevant, as it enables rapid, non-destructive assessment of antioxidant potential and batch-to-batch consistency and should be viewed as complementary to targeted analytical approaches used for propolis standardization.

Conclusion

This study presents an unbiased spectroscopic approach to screen the chemical composition of propolis from Australia, Denmark, and Norway using multiple spectroscopic techniques, and to predict antioxidative activity (expressed as DPPH RSA) in the Scandinavian samples based on Raman, NIR, and ^{1}H NMR spectroscopy. PCA showed no significant differences between Danish and Norwegian propolis, both of which had higher aromatic content than Australian samples, whereas the latter was richer in carbohydrates and terpenoids. Australian propolis also exhibited significantly lower RSA compared to Danish and Norwegian samples. Across all applied techniques, the strongest correlations with RSA were observed at 1631 cm^{-1} in Raman and 1666 nm in NIR, linked to conjugated C=C and first overtones of aromatic/conjugated C-H stretches, respectively. NIR spectroscopy yielded the most accurate RSA predictions (R^2 = 0.75, RMSECV = 6.66%), followed by ^{1}H NMR and Raman, while IR was less predictive. Thus, NIR, in particular, shows strong potential as a rapid, non-destructive tool for routine quality control of chemically complex natural products such as propolis. The results also clearly demonstrate the complementary nature of the applied spectroscopic techniques, as Raman exhibited sensitivity to aromatic features linked to RSA, IR provided broad functional-group information, and NIR captured both aromatic signatures and a more holistic chemical overview. In addition, 2D correlations with ^{1}H NMR spectroscopy enhanced the interpretation across the different techniques.

Finally, the clear compositional and functional differences between Australian and Scandinavian propolis highlight the strong influence of geographical and botanical variability on propolis chemistry and its associated bioactivity.

CRediT authorship contribution statement

Hasim Tekin: Writing – review & editing, Methodology, Funding acquisition, Conceptualization. **Julie Christine Antvorskov:** Writing – review & editing, Supervision, Project administration, Funding acquisition, Conceptualization. **Søren Balling Engelsen:** Writing – review & editing, Visualization, Supervision, Methodology, Data curation, Conceptualization. **Knud Josefsen:** Writing – review & editing, Supervision, Methodology, Funding acquisition, Data curation, Conceptualization. **Jonas Pordel Vind:** Writing – review & editing, Writing – original draft, Project administration, Data curation. **Henrik Munch Jørgensen:** Writing – review & editing, Supervision, Project administration, Funding acquisition. **Violetta Aru:** Writing – review & editing, Supervision, Methodology, Data curation.

Declaration of Competing Interest

The authors declare that they have no known competing financial interests or personal relationships that could have appeared to influence the work reported in this paper.

Funding/Acknowledgement

This work was funded by the European Union and the Danish Agricultural Agency under the national implementation of the Apiculture Support Scheme 2023–2026. Data was generated though accessing research infrastructure at the University of Copenhagen, including FOODHAY (Food and Health Open Innovation Laboratory, Danish

Roadmap for Research Infrastructure).

Appendix A. Supporting information

Supplementary data associated with this article can be found in the online version at doi:10.1016/j.prenap.2026.100578.

Data availability

Data will be made available on request.

References

[1] M. Simone-Finstrom, M. Spivak, Propolis and bee health: the natural history and significance of resin use by honey bees, Apidologie 41 (3) (2010) 295–311, https://doi.org/10.1051/apido/2010016.

[2] E.L. Ghisalberti, Propolis: A Review, Bee World 60 (2) (1979) 59–84, https://doi.org/10.1080/0005772X.1979.11097738.

[3] R. Hossain, C. Quispe, R.A. Khan, A.S.M. Saikat, P. Ray, D. Ongalbek, et al., Propolis: an update on its chemistry and pharmacological applications, Chin. Med. 17 (1) (2022) 100, https://doi.org/10.1186/s13020-022-00651-2.

[4] N. Drescher, A.M. Klein, T. Schmitt, S.D. Leonhardt, A clue on bee glue: new insight into the sources and factors driving resin intake in honeybees (Apis mellifera), PLoS One 14 (2) (2019) e0210594, https://doi.org/10.1371/journal.pone.0210594.

[5] M. Dobrosielska, R. Dobrucka, P. Kozera, D. Brząkalski, E. Gabriel, J. Głowacka, et al., Beeswax as a natural alternative to synthetic waxes for fabrication of PLA/diatomaceous earth composites, Sci. Rep. 13 (1) (2023) 1161, https://doi.org/10.1038/s41598-023-28435-0.

[6] J. Cuní, P. Cuni, B. Eisen, R. Savizky, J. Bové, Characterization of the binding medium used in Roman encaustic paintings on wall and wood, Anal. Methods 4 (2012) 659–669, https://doi.org/10.1039/C2AY05635F.

[7] A. Kurek-Górecka, Ş. Keskin, O. Bobis, R. Felitti, M. Górecki, M. Otręba, et al., Comparison of the Antioxidant Activity of Propolis Samples from Different Geographical Regions, Plants 11 (9) (2022), https://doi.org/10.3390/plants11091203.

[8] M.L.F. Bittencourt, P.R. Ribeiro, R.L.P. Franco, H.W.M. Hilhorst, R.D. de Castro, L. G. Fernandez, Metabolite profiling, antioxidant and antibacterial activities of Brazilian propolis: Use of correlation and multivariate analyses to identify potential bioactive compounds, Food Res. Int. 76 (2015) 449–457, https://doi.org/10.1016/j.foodres.2015.07.008.

[9] S.M. Osés, P. Marcos, P. Azofra, A. de Pablo, M. Fernández-Muíño, M.T. Sancho, Phenolic profile, antioxidant capacities and enzymatic inhibitory activities of propolis from different geographical areas: needs for analytical harmonization, Antioxidants 9 (1) (2020), https://doi.org/10.3390/antiox9010075.

[10] L. Barrientos, C.L. Herrera, G. Montenegro, X. Ortega, J. Veloz, M. Alvear, et al., Chemical and botanical characterization of Chilean propolis and biological activity on cariogenic bacteria Streptococcus mutans and Streptococcus sobrinus, Braz. J. Microbiol 44 (2) (2013) 577–585, https://doi.org/10.1590/s1517-83822013000200038.

[11] Y. Zhang, C. Cao, Z. Yang, G. Jia, X. Liu, X. Li, et al., Simultaneous determination of 20 phenolic compounds in propolis by HPLC-UV and HPLC-MS/MS, J. Food Compos. Anal. 115 (2023) 104877, https://doi.org/10.1016/j.jfca.2022.104877.

[12] B. Khakimov, G. Gürdeniz, S. Engelsen, Trends in the application of chemometrics to foodomics studies, Acta Aliment. 44 (2015) 4–31, https://doi.org/10.1556/AAlim.44.2015.1.1.

[13] M. Surek, Ad.F. Cobre, M.M. Fachi, T.G. Santos, R. Pontarolo, A.R. Crisma, et al., Propolis authentication of stingless bees by mid-infrared spectroscopy and chemometric analysis, LWT 161 (2022) 113370, https://doi.org/10.1016/j.lwt.2022.113370.

[14] I. Revilla, A.M. Vivar-Quintana, I. González-Martín, O. Escuredo, C. Seijo, The potential of near infrared spectroscopy for determining the phenolic, antioxidant, color and bactericide characteristics of raw propolis, Microchem. J. 134 (2017) 211–217, https://doi.org/10.1016/j.microc.2017.06.006.

[15] M.I. Stavropoulou, K. Stathopoulou, A. Cheilari, D. Benaki, K. Gardikis, I. Chinou, et al., NMR metabolic profiling of Greek propolis samples: Comparative evaluation of their phytochemical compositions and investigation of their anti-ageing and antioxidant properties, J. Pharm. Biomed. Anal. 194 (2021) 113814, https://doi.org/10.1016/j.jpba.2020.113814.

[16] S. Kumazawa, K. Hayashi, K. Kajiya, T. Ishii, T. Hamasaka, T. Nakayama, Studies of the constituents of uruguayan propolis, J. Agric. Food Chem. 50 (17) (2002) 4777–4782, https://doi.org/10.1021/jf020279y.

[17] Å. Rinnan, M. Andersson, C. Ridder, S.B. Engelsen, Recursive weighted partial least squares (rPLS): an efficient variable selection method using PLS, J. Chemom. 28 (5) (2014) 439–447, https://doi.org/10.1002/cem.2582.

[18] L.A. Mărghitaş, D. Dezmirean, A. Moise, C.M. Mihai, L. Laslo, DPPH method for evaluation of propolis antioxidant activity, Bull. USAMV 66 (2009) 253–258.

[19] M.M. Nichitoi, A.M. Josceanu, R.D. Isopescu, G.O. Isopencu, E.-I. Geana, C. T. Ciucure, et al., Polyphenolics profile effects upon the antioxidant and antimicrobial activity of propolis extracts, Sci. Rep. 11 (1) (2021) 20113, https://doi.org/10.1038/s41598-021-97130-9.

[20] S.B. Kedare, R.P. Singh, Genesis and development of DPPH method of antioxidant assay, J. Food Sci. Technol. 48 (4) (2011) 412–422, https://doi.org/10.1007/s13197-011-0251-1.

[21] F. Savorani, G. Tomasi, S.B. Engelsen, icoshift: A versatile tool for the rapid alignment of ^{1}D NMR spectra, J. Magn. Reson 202 (2) (2010) 190–202, https://doi.org/10.1016/j.jmr.2009.11.012.

[22] F.E. Barton, D.S. Himmelsbach, J.H. Duckworth, M.J. Smith, Two-dimensional vibration spectroscopy: correlation of mid- and near-infrared regions, Appl. Spectrosc. 46 (3) (1992) 420–429, https://doi.org/10.1366/0003702924125375.

[23] I. Noda, Generalized two-dimensional correlation method applicable to infrared, Raman, and other types of spectroscopy, Appl. Spectrosc. 47 (9) (1993) 1329–1336.

[24] R.J. Barnes, M.S. Dhanoa, S.J. Lister, Standard normal variate transformation and de-trending of near-infrared diffuse reflectance spectra, Appl. Spectrosc. 43 (5) (1989) 772–777, https://doi.org/10.1366/0003702894202201.

[25] S. Wold, K. Esbensen, P. Geladi, Principal component analysis, Chemom. Intell. Lab. Syst. 2 (1) (1987) 37–52, https://doi.org/10.1016/0169-7439(87)80084-9.

[26] The multivariate calibration problem in chemistry solved by the PLS method, in: S. Wold, H. Martens, H. Wold (Eds.), Matrix Pencils, Springer, Berlin, Heidelberg, 1983.

[27] E. Wiercigroch, E. Szafraniec, K. Czamara, M.Z. Pacia, K. Majzner, K. Kochan, et al., Raman and infrared spectroscopy of carbohydrates: a review, Spectrochim. Acta Part A Mol. Biomol. Spectrosc. 185 (2017) 317–335, https://doi.org/10.1016/j.saa.2017.05.045.

[28] B.M. Mitzner, V.J. Mancini, S. Lemberg, E.T. Theimer, Infrared spectra of monoterpenes and related compounds. II. Terpene alcohols, Appl. Spectrosc. 22 (1) (1968) 34–53.

[29] A. Hassabo, Saturated fatty acids derivatives as assistants materials for textile processes, J. Text. Sci. & Fash. Technol. 1 (2018), https://doi.org/10.33552/JTSFT.2018.01.000516.

[30] M. Krysa, M. Szymańska-Chargot, A. Zdunek, FT-IR and FT-Raman fingerprints of flavonoids - a review, Food Chem. 393 (2022) 133430, https://doi.org/10.1016/j.foodchem.2022.133430.

[31] H.G.M. Edwards, D.W. Farwell, L. Daffner, Fourier-transform Raman spectroscopic study of natural waxes and resins. I, Spectrochim. Acta Part A Mol. Biomol. Spectrosc. 52 (12) (1996) 1639–1648, https://doi.org/10.1016/0584-8539(96)01730-8.

[32] C. Corredor, T. Teslova, M.V. Cañamares, Z. Chen, J. Zhang, J.R. Lombardi, et al., Raman and surface-enhanced Raman spectra of chrysin, apigenin and luteolin, Vib. Spectrosc. 49 (2) (2009) 190–195, https://doi.org/10.1016/j.vibspec.2008.07.012.

[33] Majhi A. Himanshu, B. Behera, Prediction of wax content in crude oil and petroleum fraction by proton NMR, Pet. Sci. Technol. 37 (2018) 1–8, https://doi.org/10.1080/10916466.2018.1536713.

[34] A.G. Abdul Jameel, Identification and quantification of hydrocarbon functional groups in gasoline using (1)H NMR spectroscopy for property prediction, Molecules 26 (22) (2021), https://doi.org/10.3390/molecules26226989.

[35] I. Noda, A.E. Dowrey, C. Marcott, G.M. Story, Y. Ozaki, Generalized two-dimensional correlation spectroscopy, Appl. Spectrosc. 54 (7) (2000) 236A–248AA, https://doi.org/10.1366/0003702001950454.

[36] A.B. Brizuela, L.C. Bichara, E. Romano, A. Yurquina, S. Locatelli, S.A. Brandán, A complete characterization of the vibrational spectra of sucrose, Carbohydr. Res. 361 (2012) 212–218, https://doi.org/10.1016/j.carres.2012.07.009.

[37] G.E. McManis, L.E. Gast, IR spectra of long chain vinyl derivatives, J. Am. Oil Chem. Soc. 48 (11) (1971) 668–673, https://doi.org/10.1007/BF02638515.

[38] L. Svečnjak, G. Baranović, M. Vinceković, S. Prđun, D. Bubalo, I. Tlak Gajger, An approach for routine analytical detection of beeswax adulteration using FTIR-ATR spectroscopy, J. Apic. Sci. 59 (2015), https://doi.org/10.1515/JAS-2015-0018.

[39] O. Abbas, G. Compère, Y. Larondelle, D. Pompeu, H. Rogez, V. Baeten, Phenolic compound explorer: a mid-infrared spectroscopy database, Vib. Spectrosc. 92 (2017) 111–118, https://doi.org/10.1016/j.vibspec.2017.05.008.

[40] D. Wu, X. Chen, P. Shi, S. Wang, F. Feng, Y. He, Determination of α-linolenic acid and linoleic acid in edible oils using near-infrared spectroscopy improved by wavelet transform and uninformative variable elimination, Anal. Chim. Acta 634 (2) (2009) 166–171, https://doi.org/10.1016/j.aca.2008.12.024.

[41] M.V. Reboucas, B. de Barros Neto, Near infrared spectroscopic prediction of physical properties of aromatics-rich hydrocarbon mixtures, J. Infrared Spectrosc. 9 (4) (2001) 263–273, https://doi.org/10.1255/jnirs.312.

[42] L.G. Weyer, S.C. Lo, Spectra– structure correlations in the near-infrared, Handb. Vib. Spectrosc. (2006).

[43] M. Barea-Sepúlveda, J.L.P. Calle, M. Ferreiro-González, M. Palma, Rapid classification of petroleum waxes: a Vis-NIR spectroscopy and machine learning approach, Foods 12 (18) (2023), https://doi.org/10.3390/foods12183362.

[44] M. Baglioni, G. Poggi, G. Ciolli, E. Fratini, R. Giorgi, P. Baglioni, A triton X-100-based microemulsion for the removal of hydrophobic materials from works of art: SAXS characterization and application, Mater. (Basel) 11 (7) (2018), https://doi.org/10.3390/ma11071144.

[45] T.P. Czaja, S.B. Engelsen, Why nothing beats NIRS technology: the green analytical choice for the future sustainable food production, Spectrochim. Acta Part A Mol. Biomol. Spectrosc. 325 (2025) 125028, https://doi.org/10.1016/j.saa.2024.125028.

[46] S. Baliyan, R. Mukherjee, A. Priyadarshini, A. Vibhuti, A. Gupta, R.P. Pandey, et al., Determination of antioxidants by DPPH radical scavenging activity and quantitative phytochemical analysis of Ficus religiosa, Molecules 27 (4) (2022), https://doi.org/10.3390/molecules27041326.

[47] E. Berger, H.-P. Komsa, Polarizability models for simulations of finite temperature Raman spectra from machine learning molecular dynamics, Phys. Rev. Mater. 8 (4) (2024) 043802, https://doi.org/10.1103/PhysRevMaterials.8.043802.
[48] Å. Rinnan, F. Berg, S. Engelsen, Review of the most common pre-processing techniques for near-infrared spectra, TrAC Trends Anal. Chem. 28 (2009) 1201–1222, https://doi.org/10.1016/j.trac.2009.07.007.
[49] L.R. Bernal-Alvarez, P.E. Martinez-Munoz, A.M. Castillo-Paz, H.D. Garcia-Vazquez, B.M. Millán-Malo, M.E. Rodriguez-Garcia, Infrared spectroscopy as a tool to study the vibrational, mechanical, and structural changes in commercial plastic bags: physical principles, J. Mol. Struct. 1303 (2024) 137580, https://doi.org/10.1016/j.molstruc.2024.137580.
[50] L. Zhu, J. Zhang, H. Yang, G. Li, H. Li, Z. Deng, et al., Propolis polyphenols: a review on the composition and anti-obesity mechanism of different types of propolis polyphenols, Front. Nutr. 10 (2023), https://doi.org/10.3389/fnut.2023.1066789.